Proton pygmy dipole resonances in ^{17,18}Ne: Collective versus noncollective excitations

Hai-Liang Ma,* Bao-Guo Dong, Yu-Liang Yan, Huan-Qiao Zhang, and Xi-Zhen Zhang
Department of Nuclear Physics, China Institute of Atomic Energy, P.O. Box 275(10), Beijing 102413, China
(Received 8 February 2012; published 9 April 2012)

The proton pygmy dipole resonances (PDRs) in the proton-rich nuclei ^{17,18}Ne are investigated in the framework of the interacting shell model. The shell model with the self-consistent Skyrme-Hartree-Fock wave functions well reproduces the experimental data of the ground-state properties. The proton PDRs in the neighboring ^{17,18}Ne are predicted. However, the detailed study involving the transition densities and collectivity shows that the PDR in ^{17}Ne is highly collective and due to the oscillation of the valence protons against the interior core, while in ^{18}Ne the dipole resonance in the PDR region is noncollective and more likely to be the configuration splitting of the giant dipole resonances.

DOI: 10.1103/PhysRevC.85.044307 PACS number(s): 21.10.Gv, 21.60.Cs, 23.20.−g, 24.30.Cz

I. INTRODUCTION

The exotic behavior of nuclei approaching the drip lines is one of the top subjects in nuclear physics studies. The loosely bound nucleons can oscillate against the isospin saturated core. Large enhancement of electric dipole ($E1$) response is expected in the low-energy region, namely, the pygmy dipole resonance (PDR). Although PDR exhausts only a few percent of the total energy-weighted sum rule, nucleon capture rates could be largely enhanced in the r-process nucleosynthesis [1]. The neutron PDRs have been intensely studied in heavy and medium-heavy nuclei [2–9]. Due to the existence of the Coulomb barrier, the proton skin or halo can only appear in light nuclei and is less profound than the neutron skin or halo. And proton PDRs are much rarer than neutron PDRs [10,11]. However, the nature of PDRs is still controversial, since not only can PDRs be developed by this soft mode, but also single-particle excitation near the threshold can enhance the dipole excitations [3,12,13]. The controversy can be further shown by the fact that mean-field theories have predicted the increasing integrated strength of neutron PDRs with the increasing of the neutron excess or the neutron skin thickness [2], while experimental studies show a nontrivial dependence of the total $E1$ strength as a function of the neutron number, such as in ^{40,44,48}Ca [14,15]. In some light and heavy nuclei, relativistic and nonrelativistic theories have also predicted the low-lying strengths to be of noncollective nature [16–18].

Most of the studies on the pygmy and giant dipole resonances are based on the mean-field theory with random-phase-approximation (RPA) or quasiparticle RPA. However, mean-field theories cannot predict the mixing of different configurations, which is critical for loosely bound nuclei. The collectivity of the giant dipole resonances (GDRs) in light nuclei is less profound than in medium-heavy and heavy nuclei. Therefore the response function could distribute over several configuration-dependent peaks. For electric dipole resonances, most of the contributions come from the cross shell ($\Delta N = 1$) particle-hole excitations near the Fermi surface. Although the conventional configuration-mixing shell model is confined in a restricted valence space, it was shown that the GDRs were well reproduced with this model in light nuclei [19,20]. Another advantage of the shell model is that the pairing effect is well treated, which is very important in open-shell nuclei especially in Borromean nuclei such as ^{11}Li and ^{17}Ne. With the pygmy dipole resonances lying in the lower energy region, the fully microscopic shell-model calculations could provide more insightful prediction in light nuclei. In Refs. [21,22], shell-model studies on the neutron PDRs in light or medium nuclei were reported, with rare examples of proton PDRs [23]. The PDRs in neutron-rich oxygen isotopes predicted by the shell model [19] were confirmed experimentally [24]. However, only transition strength was given in the previous shell-model studies. Detailed transition densities and collectivity are very important to revealing the dynamics of the proton PDRs.

^{17}Ne and ^{18}Ne exhibit proton halo or skin in spite of the Coulomb barrier [25]. The Borromean ^{17}Ne is a prominent candidate for a two-proton halo, which can be regarded as an ^{15}O core in its ground state plus two protons in the d^2 or halo-like s^2 configurations. The nonresonant soft dipole mode in ^{17}Ne was predicted by a three-body model [26]. In the present paper, the pygmy dipole resonances in ^{17}Ne and ^{18}Ne are predicted in the interacting shell model. The differences of PDRs in these two nuclei are discussed when the transition densities and information on collectivity are available.

II. SHELL MODEL TRANSITION DENSITY AND TRANSITION STRENGTH

The one-body transition density (OBTD) is the standard output of the shell-model code such as OXBASH and NUSHELL@MSU [27]. The OBTDs are unrelated to the radial wave function but related to the angular momentum part between the initial and final states. Thus the transition matrix element can be given by the transition operator and the transition density can be given by the density operator using the same OBTDs. The detailed formulas are given in the following discussion.

In the second-quantized representation, the λ-rank one-body operator reads

$$\hat{O}^{\lambda}_{\mu} = \sum_{\alpha\beta} \langle \alpha | O^{\lambda}_{\mu} | \beta \rangle a^{+}_{\alpha} a_{\beta}, \tag{1}$$

*mhl624@ciae.ac.cn

where α stands for the single-particle quantum number set $(n_\alpha l_\alpha j_\alpha m_\alpha)$. In the shell-model M scheme, this operator can be written in the tensor coupled form [28]

$$\hat{O}^\lambda_\mu = \sum_{k_\alpha k_\beta} \langle k_\alpha || O^\lambda || k_\beta \rangle \frac{\left[a^+_{k_\alpha} \otimes \tilde{a}_{k_\beta}\right]^\lambda_\mu}{\sqrt{2\lambda+1}}, \quad (2)$$

where k_α stands for $(n_\alpha l_\alpha j_\alpha)$. The reduced transition matrix element between the final state $|J_f\rangle$ and initial state $|J_i\rangle$ can be expressed by the OBTDs and reduced single-particle matrix elements of the valence orbitals,

$$\langle J_f || \hat{O}^\lambda || J_i \rangle = \sum_{k_\alpha k_\beta} \mathrm{OBTD}(f i k_\alpha k_\beta \lambda) \langle k_\alpha || \hat{O}^\lambda || k_\beta \rangle, \quad (3)$$

where J_i and J_f include all the quantum numbers needed to distinguish the states, and OBTD is given by

$$\mathrm{OBTD}(f i k_\alpha k_\beta \lambda) = \frac{\langle J_f || \left[a^+_{k_\alpha} \otimes \tilde{a}_{k_\beta}\right]^\lambda || J_i \rangle}{\sqrt{2\lambda+1}}. \quad (4)$$

The OBTD can also be defined to include the isospin freedom [28].

The transition density between the final state $|J_f\rangle$ and initial state $|J_i\rangle$ is defined as

$$\delta\rho(\vec{r}) = \langle J_f | \sum_i \delta(\vec{r} - \vec{r}_i) | J_i \rangle, \quad (5)$$

and the radial transition density $\delta\rho_\lambda(r)$ is given by

$$\delta\rho(\vec{r}) \equiv \sum_{\lambda,\mu} \delta\rho_\lambda(r) Y_{\lambda\mu}(\hat{r}). \quad (6)$$

Using the orthonormal relation of spherical harmonics, we have

$$\delta\rho_\lambda(r) = \int \langle J_f | \sum_i \delta(\vec{r} - \vec{r}_i) | J_i \rangle Y^*_{\lambda\mu}(\hat{r}) d\Omega. \quad (7)$$

As $\delta(\vec{r} - \vec{r}_i) = \frac{1}{4\pi r^2}\delta(r - r_i)\delta(\hat{r}, \hat{r}_i)$, by integrating out the angular part, we have

$$\delta\rho_\lambda(r) \sim \frac{\langle J_f || \sum_i \frac{1}{r^2}\delta(r - r_i) Y_\lambda || J_i \rangle}{\sqrt{2J_i+1}}. \quad (8)$$

In order to normalize the radial transition density to the transition strength, we leave out the coefficient in front of Eq. (8) and redefine it as

$$\begin{aligned}\delta\rho_\lambda(r) &\equiv \frac{\langle J_f || \sum_i \frac{1}{r^2}\delta(r - r_i) Y_\lambda || J_i \rangle}{\sqrt{2J_i+1}} \\ &= \frac{1}{\sqrt{2J_i+1}} \sum_{k_\alpha, k_\beta} \mathrm{OBTD}(f i k_\alpha k_\beta \lambda) \\ &\quad \times \langle k_\alpha | \left| \frac{1}{r^2}\delta(r - r') Y_\lambda \right| | k_\beta \rangle, \end{aligned} \quad (9)$$

where

$$\langle k_\alpha | \left| \frac{1}{r^2}\delta(r - r') Y_\lambda \right| | k_\beta \rangle = \psi_{k_\alpha}(r) \psi_{k_\beta}(r) \langle k_\alpha || Y_\lambda || k_\beta \rangle, \quad (10)$$

and $\psi_{k_\alpha}(r)$ is the radial wave function of the valence orbital k_α. For a λ-rank one-body transition operator,

$$\hat{O}^\lambda_\mu(\vec{r}) = r^\lambda Y_{\lambda\mu}(\hat{r}), \quad (11)$$

using Eqs. (3) and (9), the electric reduced transition probability $B(E\lambda)$ is readily expressed with the proton radial transition densities,

$$B(E\lambda, i \to f) = \frac{|\langle J_f || \hat{O}^\lambda || J_i \rangle|^2}{2J_i+1} = \left[\int e \delta\rho^p_\lambda(r) r^{\lambda+2} dr \right]^2. \quad (12)$$

However, since the effective charges are frequently used in the calculation of $B(E\lambda)$, Eq. (12) should be modified accordingly using both proton and neutron transition densities,

$$B(E\lambda, i \to f) = \left[\int \left[e^{\mathrm{eff}}_p \delta\rho^p_\lambda + e^{\mathrm{eff}}_n \delta\rho^n_\lambda \right] r^{\lambda+2} dr \right]^2, \quad (13)$$

where e^{eff}_p and e^{eff}_n are the effective charges of protons and neutrons, respectively.

III. RESULTS AND DISCUSSION

In the present shell-model calculations, the NUSHELL@MSU code [27] with the WBP10 effective interaction [29] in the *spsdpf* model space, is used. The Warburton-Brown interaction WBP was originally constructed by fitting the energy levels in the $0\hbar\omega$–$1\hbar\omega$ space. In the WBP10 interaction, the coupling between the following multi-$\hbar\omega$ configurations is cut off, i.e., the two-body matrix elements for the 1p-1h $2\hbar\omega$ excitations are all set equal to 0 due to the Hartree-Fock condition. The cross shell $2\hbar\omega$ two-body matrix elements between $0s^2$ and $0p^2$ are also set equal to 0. The WBP10 interaction is enclosed in the NUSHELL@MSU package. The standard Lawson method is used to remove the center-of-mass spurious components in the wave function by adding a fictitious Hamiltonian which acts only on the center-of-mass excitation [30]. In the present calculation, the $0\hbar\omega$–$1\hbar\omega$ configuration space is adopted. Our calculation shows that the whole picture of the calculated $E1$ response function is similar if the $2\hbar\omega$–$3\hbar\omega$ configurations are included, also see the discussion in Ref. [22].

The s^2 occupation probability of the ground state in ^{17}Ne is very controversial in theoretical predictions [25,26]. Three-body cluster theory predicted a large s^2 component and therefore a halo-like structure. However, the analysis based on the Coulomb displacement energies [31,32] or the magnetic moment [33] suggested a smaller s^2 component. In Table I the ground-state properties in ^{17,18}Ne calculated by the shell model are compared with the experimental data and fermion molecular dynamic (FMD) model results. Obviously for the nuclei near the drip lines, it is not appropriate to use the harmonic wave functions but Wood-Saxon or mean-field wave functions [19,34] when calculating physical properties involving single-particle radial wave functions. In our calculations, the self-consistent Skyrme-Hartree-Fock (SHF) wave functions with the SkM* interaction [35] are used in the evaluation of nuclear radii and electric transition

TABLE I. Mass and charge radii in ^{17,18}Ne. SM(HO) and SM(HF) denote the shell-model results using the harmonic oscillator and Hartree-Fock single-particle wave functions.

A	J^π	Proton s^2 probability		δ_{pn}[a] (fm)			Mass radii (fm)				Charge radii (fm)			
		FMD	SM	FMD	SM(HO)	SM(HF)	Expt.	FMD	SM(HO)	SM(HF)	Expt.	FMD	SM(HO)	SM(HF)
17	$1/2^-_{\text{g.s.}}$	42%	23.6%	0.45	0.17	0.43	2.75(7)	2.75	2.78	2.86	3.042(21)	3.04	2.85	3.02
18	$0^+_{\text{g.s.}}$	15%	15.0%		0.15	0.25	2.81(14)	2.70	2.78	2.82	2.971(20)	2.93	2.85	2.93

[a] $\delta_{pn} = \sqrt{\langle r^2\rangle_p} - \sqrt{\langle r^2\rangle_n}$.

matrix elements. The wave functions of positive energy states are obtained by the box approximation. When the harmonic oscillator wave function is used, the parameter $b = 1.8$ fm is adopted, which is slightly larger than the value $b = \sqrt{41.4/\hbar\omega}$ where $\hbar\omega$ is the global fit $\hbar\omega \approx 45A^{-1/3}$–$25A^{-2/3}$ [36]. Clearly from Table I, the shell model with the SHF wave functions reproduces well the mass radii and charge radii both in ^{17,18}Ne. In Fig. 1 the calculated nucleon and matter density distributions are compared with the available experimental data. It is worth noting that the halo nucleon can appear in the classically forbidden region for the halo nuclei [37]. In the present calculations, the probabilities of finding one proton at $r > 5$ fm is 41% and 28% in ^{17,18}Ne, respectively. In ^{17}Ne, this probability is close to the FMD prediction of 40%. Thus by employing the more realistic radial wave functions, the halo-like structure in ^{17}Ne is reproduced in the shell model without changing the composition of configurations.

To further remove the additional spurious components due to the usage of the Skyrme-Hartree-Fock wave functions, the center-of-mass removed dipole operator is used [38] in the calculation of the dipole transition strength,

$$\tilde{Q}^{\lambda=1}_{\mu} = e\frac{N}{A}\sum_i^Z r_i Y_{1\mu}(\hat{r}_i) - e\frac{Z}{A}\sum_i^N r_i Y_{1\mu}(\hat{r}_i), \qquad (14)$$

where Z, N, and A are proton, neutron, and mass number, respectively. The effectiveness of this method was demonstrated in Ref. [19]. To smooth out the discrete strengths, the transition strengths are averaged by a Lorentz-type factor $\rho(\omega)$,

$$\frac{d\bar{B}(E1;\omega)}{d\omega} = \int \sum_n B(E1;\omega_n)\rho(\omega-\omega_n)d\omega, \qquad (15)$$

where ω is the phonon energy and

$$\rho(\omega-\omega_n) = \frac{1}{\pi}\frac{\Gamma/2}{(\omega-\omega_n)^2+\Gamma^2/4}. \qquad (16)$$

The arbitrary total width $\Gamma = 1$ MeV is chosen. In this way, the response function is like the superposition of many isolated Breit-Wigner resonances.

The electric dipole response functions and the $B(E1)$ values of discrete transitions in ^{17,18}Ne are shown in Fig. 2. We

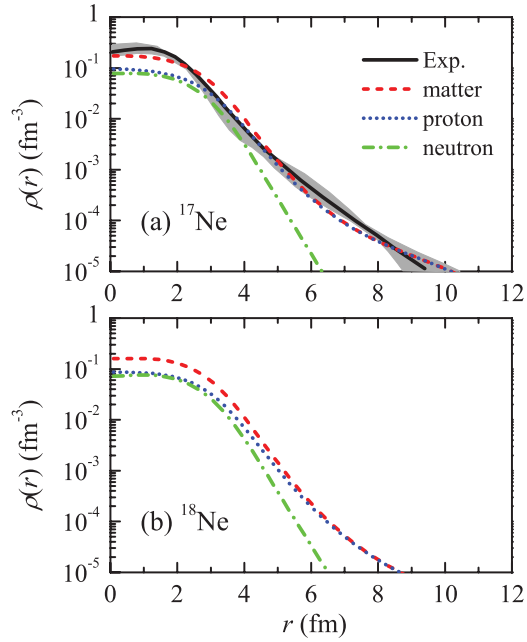

FIG. 1. (Color online) Nucleon and matter density distributions of the ground states in ^{17,18}Ne. The experimental errors are indicated by the gray area.

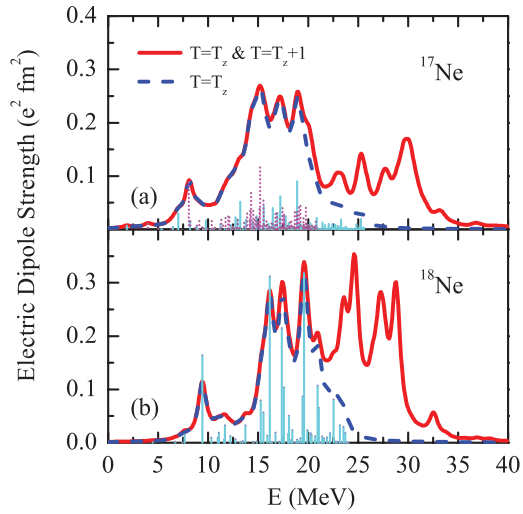

FIG. 2. (Color online) Electric dipole response functions from the excited states to the ground state in ^{17,18}Ne with the Skyrme-Hartree-Fock single-particle wave functions. The thin lines are the $B(E1, T = T_z)$ values of discrete transitions in the shell-model calculations, with the solid-cyan lines representing the $J^\pi = 1/2^+(J^\pi = 1^-)$ states in ^{17}Ne (^{18}Ne), the dotted-magenta lines representing the $J^\pi = 3/2^+$ states in ^{17}Ne.

have included the contribution from $T = T_z$ and $T = T_z + 1$ states in order to give the energy-weighted sum rule (EWSR) which is comparable with the Thomas-Reiche-Kuhn (TRK) sum rule. As an odd-A nucleus, the level density in ^{17}Ne is much higher than in even-A ^{18}Ne, so the isovector dipole transition strengths in ^{17}Ne are more spread out than in ^{18}Ne. The shell model predicts two levels in ^{17}Ne and one level in ^{18}Ne with strong $E1$ transitions around 10 MeV, which will give appreciable pygmy resonances. In ^{17}Ne, the shell model also predicts a very low $J^\pi = 1/2^+$ state at $E = 1.87$ MeV, which is 0.39 MeV above the proton emission threshold. A $B(E1)$ value of 0.00277 fm^2 could indicate some importance for the astrophysical $2p$ capture of ^{15}O in the hot CNO cycle. For ^{18}Ne, the recent study using the approach of Hartree-Fock-Bogoliubov + quasiparticle random-phase-approximation (HFB + QRPA) with the Gogny force did not predict a PDR around 10 MeV [39]. Although the pairing was included, their calculations gave the lowest resonance at 14.2 MeV, whose transition densities behave more closely to the giant dipole resonance. For ^{18}O, the mirror nucleus of ^{18}Ne, several peaks around 10 MeV were already observed [40,41]. Only with phonon coupling to the resonance included, the QRPA plus phonon coupling model can give some strength around 10 MeV in ^{18}O [16].

The sum rule is a useful measure of the collectivity of the giant resonances. For the isovector GDR, the classical energy-weighted sum rule is given by

$$S_{\rm TRK} = \sum_n \hbar\omega_n \left|\langle n|\hat{O}_\mu^{\lambda=1}|{\rm g.s.}\rangle\right|^2 = \frac{\hbar^2}{2m}\frac{9}{4\pi}\frac{NZ}{A} = 14.9\frac{NZ}{A}e^2 \ ({\rm MeV\,fm^2}), \quad (17)$$

neglecting the contributions of exchange terms. This is known as the Thomas-Reiche-Kuhn (TRK) sum rule. There is another sum rule, named the energy-weighted cluster sum rule which can be viewed as a measure of the adiabaticity between the giant and pygmy resonances [22,42]. Assuming that the nucleus (A, Z) can be decomposed into two clusters with (A_1, Z_1) and (A_2, Z_2), the cluster sum rule is given by

$$S_{\rm cluster} = \frac{\hbar^2}{2m}\frac{9}{4\pi}\frac{(Z_1A_2 - Z_2A_1)^2}{AA_1A_2}. \quad (18)$$

Table II gives the sum rules of PDRs and GDRs in ^{17,18}Ne. Since the high-lying $T = T_z + 1$ states do not contribute to the response functions in the pygmy region, only the $T = T_z$ states are included in the lower table. Using $E = 12$ MeV as a cut energy, the pygmy resonances exhaust 4.9% and 3.1% of the total sum rules in ^{17,18}Ne, respectively. In the FMD calculations, ^{17,18}Ne can be interpreted essentially as the ^{15}O or ^{16}O cores plus two protons found mainly in the s^2 or d^2 configurations [25]. If assuming the two protons as the valence nucleons and other nucleons as the core, the pygmy resonances will exhaust 56.7% and 39.1% of the cluster sum rules in ^{17,18}Ne, respectively.

TABLE II. Ground-state spins, energy-weighted sum rule (EWSR) values of $E1$ transitions in ^{17,18}Ne. The values are obtained by summing up to $E_x = 40$ MeV. The cluster sum rules are obtained assuming that the valence cluster has $Z = 2$, $A = 2$.

Nuclides	$J^\pi_{\rm g.s.}$	T	EWSR (MeV e^2 fm^2)	$S_{\rm TRK}$ (MeV e^2 fm^2)	$\frac{\rm EWSR}{S_{\rm TRK}}$ (%)
^{17}Ne	$1/2^-$	3/2	36.7		
		5/2	30.2		
		Total	66.9	61.4	109
^{18}Ne	0^+	1	35.8		
		2	47.0		
		Total	82.8	66.2	125
Nuclides	$J^\pi_{\rm g.s.}$	T	EWSR(pygmy) (MeV e^2 fm^2)	$S_{\rm cluster}$ (MeV e^2 fm^2)	$\frac{\rm EWSR(pygmy)}{S_{\rm cluster}}$ (%)
^{17}Ne	$1/2^-$	3/2	3.25	5.73	56.7
^{18}Ne	0^+	1	2.59	6.62	39.1

Although the transition strengths in ^{17,18}Ne seem to be similar, only the detailed information, i.e., transition densities, can give the possible differences between them. In the previous shell-model studies, the transition densities of the pygmy resonances and GDRs were not included [19,21–23]. Using the formulas discussed above, the calculated transition densities of the typical resonance states in ^{17,18}Ne are shown in Fig. 3. Figures 3(a) and 3(b) are for the dominant states of ^{17}Ne in the usual pygmy region. We can see that the proton and neutron move in phase in the nuclear interior, while only protons move in the exterior. This scenario is the typical pygmy resonances of the halo protons oscillating against the inner core. The state in Fig. 3(c) is located in the GDR region. The given transition densities have shown a typical oscillation in the opposite phase between the bulk protons and neutrons. There is no contribution from either protons or neutrons in the exterior region. For comparison, the transition densities of two states in the PDR region of ^{18}Ne are displayed in Figs. 3(d) and 3(e). Although the behavior in Fig. 3(d) is somewhat similar to that in Figs. 3(a) and 3(b), the peaks of proton and neutron transition densities are out of phase by about 0.9 MeV. And the $B(E1)$ value of this state is too small when compared with the state at $E = 9.413$ MeV, not to mention the dominant GDR states. The proton and neutron transition densities in Fig. 3(e) do not show clear-cut in-phase behavior. The interval of the proton and neutron peaks is 1.26 MeV. This state is clearly not the soft mode but more similar to the giant resonances like in Fig. 3(f), where the state is a typical GDR.

Unlike the GDR region, the level density is sparse in the PDR region. Further detailed information on the collectivity of the discrete PDR states can be obtained by viewing the contributions to the total transition matrix element from the valence orbital transitions. These contributions to the isovector operator [Eq. (14)] for the important PDR states discussed in the last paragraph are given in Fig. 4, where the horizontal axis is the single-particle excitation energies of valence orbitals. This figure shows that the dominant PDR states in ^{17}Ne have several components including the transitions $1p \leftrightarrow 2s1d$

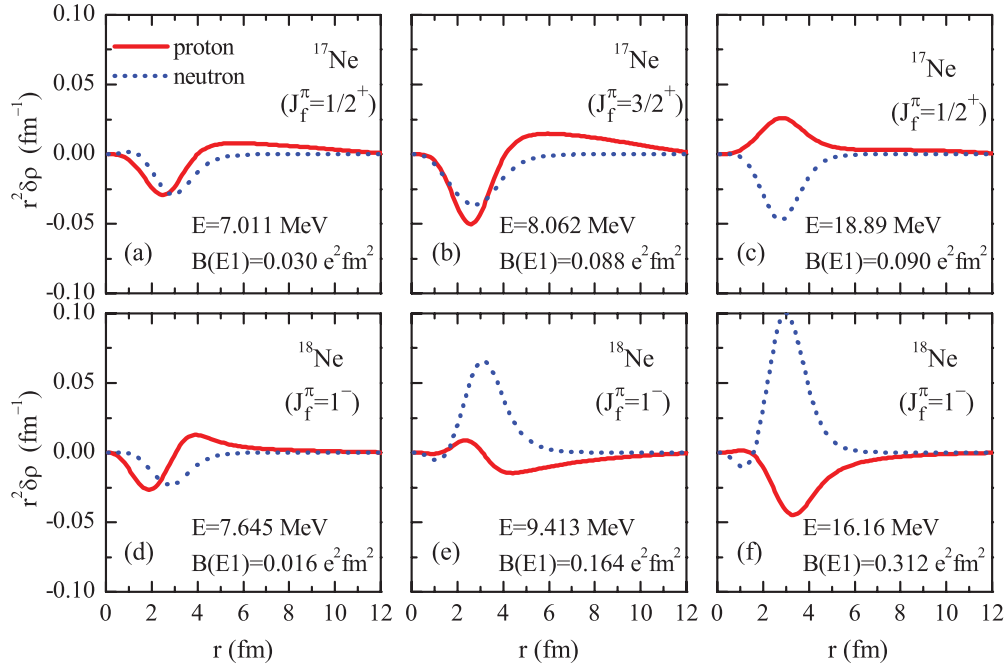

FIG. 3. (Color online) Shell-model transition densities of discrete dipole transitions in ^{17,18}Ne.

and $2s1d \leftrightarrow 1f2p$, which have prominent contributions to the total matrix elements. Together with the discussions on the transition densities, the ^{17}Ne has shown us an excellent example of collective proton PDR due to the soft mode between the valence protons and the core. However, for ^{18}Ne, the PDR states are much less collective since only a few transitions contribute, most of which comes from the $1p \leftrightarrow 2s1d$ transitions. Together with the discussions on the transition density, the nature of the $E = 9.413$ MeV state in ^{18}Ne is more likely to be the configuration splitting of the GDRs, but in the usually PDR energy region. The different nature of pygmy dipole resonances may also give a possible explanation for the nontrivial dependence of PDRs as a function of the neutron number in the Ca isotopes. Further theoretical investigations on this trend is highly needed.

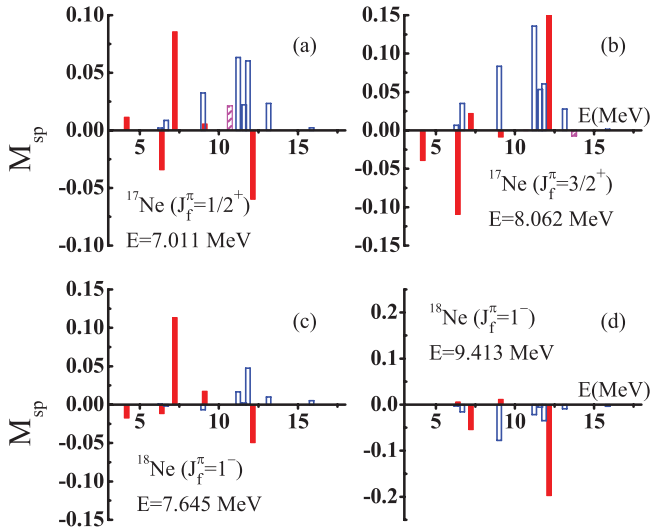

FIG. 4. (Color online) Contributions to the total matrix elements of valence orbitals for the deexcitations from PDR states in ^{17,18}Ne. The magenta bars with slanted lines, the solid red bars, and the open blue bars indicate the transitions between the valence orbitals of $1s \leftrightarrow 1p$, $1p \leftrightarrow 2s1d$, and $2s1d \leftrightarrow 1f2p$, respectively.

IV. SUMMARY

In summary, we have used the shell model to study the ground-state properties and the proton pygmy dipole resonances in ^{17,18}Ne. The shell model with the self-consistent Skyrme-Hartree-Fock wave functions reproduces well the experimental mass radii and charge radii. The mass density distributions of the ground state in ^{17}Ne also can be well given. The transition densities of the dipole resonances are calculated from the shell-model output. The pygmy resonances around 10 MeV in both ^{17,18}Ne are predicted. However, detailed study involving transition densities and collectivity shows that the PDRs in ^{17}Ne are highly collective and due to the oscillation between the valence protons and the core, while in ^{18}Ne the dipole resonance in the PDR region is noncollective and more likely to be the configuration splitting of the GDRs.

ACKNOWLEDGMENTS

The authors acknowledge the support from the NSF of China under Contracts No. 11075217, No. 11105227, and No. 11147130.

[1] S. Goriely, Phys. Lett. B **436**, 10 (1998).
[2] J. Chambers, E. Zaremba, J. P. Adams, and B. Castel, Phys. Rev. C **50**, R2671 (1994).
[3] I. Hamamoto, H. Sagawa, and X. Z. Zhang, Phys. Rev. C **57**, R1064 (1998).
[4] D. Vretenar, N. Paar, P. Ring, and G. A. Lalazissis, Phys. Rev. C **63**, 047301 (2001).
[5] N. Paar, P. Ring, T. Nikšić, and D. Vretenar, Phys. Rev. C **67**, 034312 (2003).
[6] L. G. Cao and Z. Y. Ma, Phys. Rev. C **71**, 034305 (2005).
[7] J. Liang, L. G. Cao, and Z. Y. Ma, Phys. Rev. C **75**, 054320 (2007).
[8] E. Litvinova, P. Ring, and V. Tselyaev, Phys. Rev. C **78**, 014312 (2008).
[9] J. Daoutidis and P. Ring, Phys. Rev. C **80**, 024309 (2009).
[10] N. Paar, D. Vretenar, and P. Ring, Phys. Rev. Lett. **94**, 182501 (2005).
[11] N. Paar, D. Vretenar, E. Khan, and G. Colò, Rep. Prog. Phys. **70**, 691 (2007).
[12] I. Hamamoto and X. Z. Zhang, Phys. Rev. C **58**, 3388 (1998).
[13] C. J. Lin, X. Z. Zhang, R. Zhang, Z. H. Liu, and H. Q. Zhang, Phys. Rev. C **76**, 044321 (2007).
[14] T. Hartmann, M. Babilon, S. Kamerdzhiev, E. Litvinova, D. Savran, S. Volz, and A. Zilges, Phys. Rev. Lett. **93**, 192501 (2004).
[15] J. Isaak *et al*., Phys. Rev. C **83**, 034304 (2011).
[16] G. Colò and P. F. Bortignon, Nucl. Phys. A **696**, 427 (2001).
[17] D. Sarchi, P. Bortignon, and G. Colò, Phys. Lett. B **601**, 27 (2004).
[18] D. Vretenar, N. Paar, P. Ring, and G. A. Lalazissis, Nucl. Phys. A **692**, 496 (2001).
[19] H. Sagawa and T. Suzuki, Phys. Rev. C **59**, 3116 (1999).
[20] R. A. Eramzhyan, B. S. Ishkhanov, I. M. Kapitonov, and V. G. Neudatchin, Phys. Rep. **136**, 229 (1986).
[21] H. Sagawa, T. Suzuki, H. Iwasaki, and M. Ishihara, Phys. Rev. C **63**, 034310 (2001).
[22] T. Suzuki, H. Sagawa, and K. Hagino, Phys. Rev. C **68**, 014317 (2003).
[23] C. Barbieri, E. Caurier, K. Langanke, and G. Martínez-Pinedo, Phys. Rev. C **77**, 024304 (2008).
[24] A. Leistenschneider *et al*., Phys. Rev. Lett. **86**, 5442 (2001).
[25] W. Geithner *et al*., Phys. Rev. Lett. **101**, 252502 (2008).
[26] L. Grigorenko, K. Langanke, N. Shul'gina, and M. Zhukov, Phys. Lett. B **641**, 254 (2006).
[27] B. A. Brown and W. D. M. Rae, MSU-NSCL Report, 2007.
[28] B. A. Brown, *Lecture Notes in Nuclear Structure Physics* (unpublished) [http://www.nscl.msu.edu/∼brown/Jina-workshop/BAB-lecture-notes.pdf].
[29] E. K. Warburton and B. A. Brown, Phys. Rev. C **46**, 923 (1992).
[30] D. Gloeckner and R. Lawson, Phys. Lett. B **53**, 313 (1974).
[31] H. Fortune and R. Sherr, Phys. Lett. B **503**, 70 (2001).
[32] H. T. Fortune, R. Sherr, and B. A. Brown, Phys. Rev. C **73**, 064310 (2006).
[33] W. Geithner *et al*., Phys. Rev. C **71**, 064319 (2005).
[34] D. J. Millener, J. W. Olness, E. K. Warburton, and S. S. Hanna, Phys. Rev. C **28**, 497 (1983).
[35] J. Bartel, P. Quentin, M. Brack, C. Guet, and H. B. Håkansson, Nucl. Phys. A **386**, 79 (1982).
[36] J. Blomqvist and A. Molinari, Nucl. Phys. A **106**, 545 (1968).
[37] K. Riisager, in *The Euroschool Lectures on Physics with Exotic Beams*, Lecture Notes in Physics 700, edited by J. Al-Khalili and E. Roeckl, Vol. II (Springer, Berlin, 2006), pp. 1–36.
[38] A. Bohr and B. R. Mottelson, *Nuclear Structure* (Benjamin, New York, 1975), Vol. II.
[39] M. Martini, S. Péru, and M. Dupuis, Phys. Rev. C **83**, 034309 (2011).
[40] J. G. Woodworth, K. G. McNeill, J. W. Jury, R. A. Alvarez, B. L. Berman, D. D. Faul, and P. Meyer, Phys. Rev. C **19**, 1667 (1979).
[41] H. Harada, Y. Shigetome, H. Ohgaki, T. Noguchi, and T. Yamazaki, Phys. Rev. Lett. **80**, 33 (1998).
[42] Y. Alhassid, M. Gai, and G. F. Bertsch, Phys. Rev. Lett. **49**, 1482 (1982).